PCCP

RSC Publishing

PAPER

View Article Online
View Journal | View Issue

Cite this: *Phys. Chem. Chem. Phys.*, 2013, **15**, 9862

Nanopore-type black silicon anti-reflection layers fabricated by a one-step silver-assisted chemical etching

Yen-Tien Lu[a] and Andrew R. Barron†*[bcd]

Received 30th April 2013,
Accepted 7th May 2013

DOI: 10.1039/c3cp51835c

www.rsc.org/pccp

An effective and economical fabrication process for the synthesis of nanopore-type ''black silicon'', that significantly decreases reflectivity of silicon wafer surfaces, is reported using a room temperature one-step Ag-assisted chemical etching method. The effects on the surface morphology and the corresponding surface reflectivity of the concentration of the silver catalyst (500, 50, and 5 μM), the HF and H_2O_2 concentration in the silicon etchant, the HF : H_2O_2 ratio, and etching time have been investigated. Lower reflectivity is a balance between sufficient silver catalyst to create large numbers of nanopores on a silicon surface and excessive silver that brings deeply etched channels that would potentially short-circuit a solar cell junction. The lowest relative effective reflectivity (0.17% over a range of 300–1000 nm) occurs with a silver ion concentration of 50 μM, however, with the silver ion concentration decreases to 5 μM surfaces with a low relative effective reflectivity (2.60%) and a short nanopore length (<250 nm) can be obtained with 10 minute etching time, indicating that this method can be used as a simple (one-pot), low cost (low silver concentration), energy efficient (room temperature), method for the synthesis of anti-reflection layers for silicon-based solar cell applications.

1. Introduction

Solar cells need low surface reflectance to maximize the amount of incident photons absorbed by the semiconductor to convert incident light into electrical energy. In the solar cell industry, the use of an anti-reflection (AR) coating is a popular method to suppress the reflection of solar cell surface by forming destructive interference of incident light. Typical AR coatings for silicon solar cells are SiN_x produced by chemical vapour deposition have a reflectance of about 6% as compared to 40% for a polished silicon wafer. However, AR coatings are limited in use because it only reduces the reflection for a narrow range of light wavelength and incident angle since its functionality is based on a quarter-wavelength coating.[1–4] Thus, the lowest reflectivity (and hence highest photon to electron efficiency) of a solar cell will only occur when the incident sunlight is at a particular angle. A potential replacement for the conventional AR coating, so-called ''black silicon'' (b-Si), first reported by Jansen *et al.*,[5] has attracted attention for Si-based solar cells.[6–8] Black silicon is a type of porous silicon whose surface morphology provides a graded refractive index between the silicon surface of the device and air, that results in a low reflectivity and a correspondingly high absorption of visible light.[9] Black silicon has been successfully fabricated by several different methods including reactive ion etching,[5,10,11] laser chemical etching,[12–14] pulsed electrochemical etching,[4,15] and fast atom beam etching.[16] However, these techniques need either expensive instruments and high energy consumption or complicated fabricating processes, making them unfavorable for industrial applications.

Recently, an economical and efficient approach for industrial b-Si manufacturing called metal-assisted chemical etching method has been developed to avoid the above disadvantages.[8,17–20] The metal-assisted chemical etching method includes two steps: metal deposition and electroless chemical etching. In the metal deposition step, a noble metal, such as Au, Ag, and Pt is deposited on the Si surface usually as nanoparticles (NPs).[21,22] The metal NPs attract

[a] *Department of Chemical and Biomolecular Engineering, Rice University, Houston, Texas 77005, USA*
[b] *Department of Chemistry, Rice University, Houston, Texas 77005, USA. E-mail: arb@rice.edu; Tel: +1 713 348 5610*
[c] *Department of Mechanical Engineering and Materials Science, Rice University, Houston, TX 77005, USA*
[d] *College of Engineering, Swansea University, Singleton Park, Swansea SA2 8PP, Wales, UK*

† These studies were supported by funding from Natcore Technology, Inc. This author is the scientific founder of, and has an equity interest in, Natcore Technology, Inc., a company that may potentially benefit from the research results, and also serves on the company's Scientific Advisory Board.

electrons from the silicon surface promoting the oxidation to SiO_2 in the presence of an appropriate oxidant. In the electroless chemical etching step, the as-formed SiO_2 is etched away by HF (as H_2SiF_6) and a pit is produced under each NP. As these reactions occur in a continuous process the pits become deeper and ultimately connect with each other, and remaining Si substrate forms b-Si that consists of a silicon nanowire (Si-NW) structure. Unfortunately, this nanowire structure is very fragile making the incorporation of b-Si into typical fab processes difficult.[20]

A proposed mechanism based on the working principle of galvanic cells thoroughly explains the electroless chemical etching with metal NP deposition on the Si material surface.[23] The mechanism consists of two half-cell reactions: a cathode reaction at the metal NP surface (eqn (1)) and an anode reaction occurring at the contact point between the Si and metal NP (eqn (2) and (3)).[19,22–25] The overall reaction is thus as shown in eqn (4).

$$H_2O_2 + 2H^+ + 2e^- \rightleftharpoons 2H_2O \quad (1)$$

$$Si + 2H_2O \rightleftharpoons SiO_2 + 4H^+ + 4e^- \quad (2)$$

$$SiO_2 + 6HF \rightleftharpoons H_2SiF_6 + 2H_2O \quad (3)$$

$$Si + 2H_2O_2 + 6HF \rightleftharpoons H_2SiF_6 + 4H_2O \quad (4)$$

The potential difference between the cathode sites and the anode sites results a net flux of electrons through the metal NPs and accumulation of electrons on the cathode sites. Since the cathode sites can provide more electrons for the reduction of H_2O_2, the overall reaction (eqn (4)) continues resulting in etching of Si under the Ag NPs.[23]

Branz *et al.* developed a one-step Au-assisted chemical etching method based on the two-step metal-assisted chemical etching to fabricate nanopore-type b-Si.[26] During the process of the one-step method, the deposition of Au NPs and the chemical etching of Si occurred simultaneously on the Si wafer surface within the system consisting of $HAuCl_4 : HF : H_2O_2 : H_2O$, where Au^{3+} ions were reduced to Au NPs on the Si wafer surface. The fabricated nanopore structure suppressed the reflectance of the wafer to below 2% across a wavelength range of 300–1000 nm.

Unfortunately, some porous Si structures possessing low reflectivity lead to failure in improving energy conversion efficiency of the Si-based solar cells because their surface area is too high resulting in high charge recombination. To overcome this problem Branz and co-workers demonstrated that a two step silver-assisted chemical etching to fabricate nanopores could be followed by a third step, which involves etching using tetramethylammonium hydroxide (TMAH) to shorten the nanopore length.[27] However, the concentration of silver is relatively high (1 mM) for Ag deposition and the process takes three distinct steps to accomplish the desired structure. Based on this result we are interested in two challenges: what is the effect of silver concentration and can the reaction be formed in a one-step process?

Herein, our research focuses on the one-step Ag-assisted chemical etching to fabricate b-Si, since the Ag precursor has lower cost than the Au equivalent and recycling of the Ag is well understood in the (now defunct) film industry. In our study, $AgNO_3$ was utilized as an Ag NP precursor in a $HF : H_2O_2 : H_2O$ solution to compose of a Si etchant. The H_2O_2 not only facilitates the Si etching (eqn (4)) but also reduces Ag^+ ions to Ag NPs on the Si wafer (eqn (5)).

$$2Ag^+ + H_2O_2 \rightleftharpoons O_2 + 2H^+ + 2Ag \quad (5)$$

We are interested in the effects of the Ag ion concentration and the volume ratio of $HF : H_2O_2 : H_2O$ on the morphology and reflectivity of the b-Si surface. Compared to other methods, the one-step Ag-assisted chemical etching simplifies the b-Si fabrication process and may cut down the cost of the facilities and energy expenditures, which is beneficial for industrial applications. In addition, unlike Si-NW arrays, the nanopore-type b-Si possesses no high-aspect-ratio needle-liked structure and is not as fragile as SiNW arrays and can thus better endure the stress during the solar cell assembly.

2. Experimental

All the reactions were carried out in sealed plasticware at room temperature. $AgNO_3$ (Sigma-Aldrich), HF (48%, Sigma-Aldrich), H_2O_2 (30%, EMD), and NH_4OH (30%, Fisher Scientific) were used as received. Polished single crystalline (100) p-type boron-doped Si wafers (Silicon Quest International), with resistivity of 1–5 Ω cm, were individually ultrasonically cleaned in acetone and ultra-pure DI water.

The cleaned Si pieces were etched in Si etchants containing HF (48%), H_2O_2 (30%), and ultra-pure water in different volume ratios with an equal volume of 1000, 100 and 10 μM $AgNO_3$ aqueous solutions with sonication (Table 1), giving an overall $[Ag^+]$ in the etchant of 500, 50, and 5 μM, respectively. In the text, the volume ratio is given as $X : Y : Z$ corresponding to the volume ratio of HF, H_2O_2, and H_2O in the etchant, respectively. After etching for 2, 5, 10, or 20 min, the as-prepared b-Si samples were rinsed in ultra-pure DI water, and then cleaned by a silver etchant consisting of NH_4OH and H_2O_2 in a 1 : 1 volume ratio at room temperature with sonication to remove the Ag NPs on the wafer surface. The Ag-removed samples were immersed in DI water again and dried by canned air.

The morphology and structure of b-Si samples in plane and cross section were characterized by using FEI Quanta 400 high-resolution field emission scanning electron microscope (FESEM). The Ag NP size on the Si wafer surface was characterized by using the image analysis program ImageJ. The reflectivity of b-Si samples was measured by using Ocean Optics HR2000+ high-resolution spectrometer with a Mikropack DH-2000-BAL deuterium-halogen light source.

3. Results and discussion

Using a high Ag ion concentration (500 μM) results in only Ag NPs and shallow pits being formed. However, no nanopores can be observed on the Si wafer surface. Fig. 1 shows SEM images of Ag NPs formed on the Si wafer surfaces with different $HF : H_2O_2 : H_2O$ volume ratios. We propose that no nanopores appear on the wafer

Table 1 Summary of etch solutions

$HF:H_2O_2:H_2O$	$[Ag^+]$ (μM)	Volume HF[a] (mL)	Volume H_2O_2[b] (mL)	Volume DI H_2O (mL)	Volume of mixture[d] (mL)	Volume $AgNO_3$[c] (μL)	Volume DI H_2O (mL)	Total volume (mL)
1 : 5 : 2	500	1.0	5.0	2.0	5.0	500	4.50	10.0
1 : 5 : 2	50	1.0	5.0	2.0	5.0	50.0	4.95	10.0
1 : 5 : 2	5	1.0	5.0	2.0	5.0	5.0	5.00	10.0
1 : 5 : 5	500	1.0	5.0	5.0	5.0	500	4.50	10.0
1 : 5 : 5	50	1.0	5.0	5.0	5.0	50.0	4.95	10.0
1 : 5 : 5	5	1.0	5.0	5.0	5.0	5.0	5.00	10.0
1 : 5 : 10	500	1.0	5.0	10.0	5.0	500	4.50	10.0
1 : 5 : 10	50	1.0	5.0	10.0	5.0	50.0	4.95	10.0
1 : 5 : 10	5	1.0	5.0	10.0	5.0	5.0	5.00	10.0
1 : 5 : 20	500	1.0	5.0	20.0	5.0	500	4.50	10.0
1 : 5 : 20	50	1.0	5.0	20.0	5.0	50.0	4.95	10.0
1 : 5 : 20	5	1.0	5.0	20.0	5.0	5.0	5.00	10.0
2 : 4 : 20	5	2.0	4.0	20.0	5.0	5.0	5.00	10.0
3 : 3 : 20	5	3.0	3.0	20.0	5.0	5.0	5.00	10.0
4 : 2 : 20	5	4.0	2.0	20.0	5.0	5.0	5.00	10.0
5 : 1 : 20	5	5.0	1.0	20.0	5.0	5.0	5.00	10.0

[a] 48% HF. [b] 30% H_2O_2. [c] $[AgNO_3]$ = 0.01 M. [d] HF + H_2O_2 + H_2O.

surfaces due to the fact that the majority of the surface is covered by the Ag NPs under the high $[Ag^+]$ etching conditions. In the Ag-assisted chemical etching method, the HF etches away not only the areas underneath the Ag NPs but also the areas adjacent to the Ag NPs, as may be seen by the images of the Ag NP sitting inside larger pits (Fig. 1b and c). As the majority of the wafer surface is covered by Ag NPs, a near isotropic oxidation of Si occurs. This causes different regions of the Si wafer to be subject a similar etching level and no nanopores can be observed on the Si wafers.

It was also observed that the average diameters of the Ag NPs prepared in solutions of different $HF:H_2O_2:H_2O$ ratios increase with time even at the earliest stages of the etch process. After reaching a maximum size at 5 min, the NPs gradually decrease in size. Fig. 2 shows the average diameters of Ag NPs for different etching time and $HF:H_2O_2:H_2O$ volume ratios. A reasonable explanation for this effect is that the H_2O_2 in the Si etchant not only assists the Ag NP formation but also dissolves the as-formed Ag NPs into Ag ions (eqn (6)). As the H_2O_2 has been consumed and its concentration is no longer high enough, the equilibrium is shifted; resulting in the dissolution of the Ag NPs dominates and decreases the average size of Ag NPs.

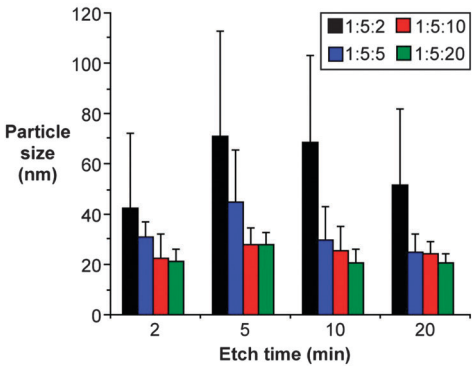

Fig. 2 Average diameter of the Ag NPs synthesized by the Si etchant containing 500 μM $[Ag^+]$ with different $HF:H_2O_2:H_2O$ ratios. The error bars represent one standard deviation of the Ag NP diameters.

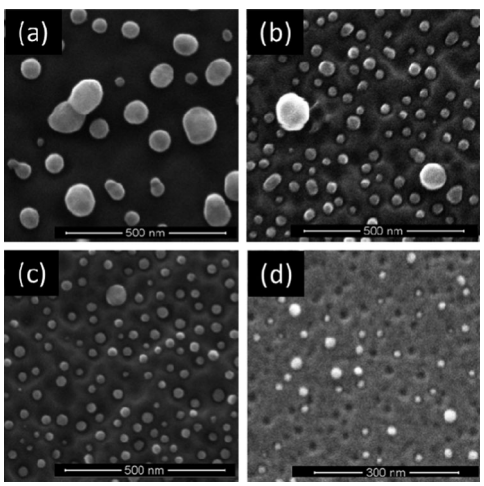

Fig. 1 SEM images of the Ag NPs on the Si wafer surfaces synthesized by the Si etchant containing 500 μM $[Ag^+]$ with 10 minutes etching and various $HF:H_2O_2:H_2O$ ratios as (a) 1 : 5 : 2, (b) 1 : 5 : 5, (c) 1 : 5 : 10, (d) 1 : 5 : 20. All scale bars = 300 nm.

$$2Ag + H_2O_2 + 2H^+ \rightleftharpoons 2Ag^+ + 2H_2O \quad (6)$$

Another observation is that with the lower [HF] and $[H_2O_2]$ the average diameter of the Ag NPs is more constant with etching time and the standard deviation in NP diameter also is smaller (Fig. 2). This indicates that the Ag NPs are smaller with a more monodispersed size, which may be attributed to the fact that a lower $[H_2O_2]$ leads a slower rate of formation of Ag NPs (eqn (5)). The slower growth rate limits the difference in Ag NP size between the earlier-formed NPs and later-formed NPs during the etching process. In addition, it implies that in order to fabricate nanopores with more uniform size distribution, relying on the lower [HF] and $[H_2O_2]$ to form monodispersed Ag NPs is necessary since the nanopores are simply the sinking track of Ag NPs.

As the Ag ion concentration is reduced to 50 μM, nanopores are observed on the Si wafer surfaces, with the majority of them being macropores (50–1000 nm). The lower [Ag^+] provides a lower nucleation and growth rate of Ag NPs; therefore, the Si wafer surface is no longer mostly covered by Ag NPs. In other words, the Ag NPs on the wafer surface are better dispersed and are able to nearly unidirectional oxidize the Si under the Ag NPs to SiO_2 which is immediately etched by HF. As long as both of the oxidation and etching continue, the Ag NPs would keep sinking into the wafer surface and increase the nanopore length. Fig. 3 shows SEM images of the morphology of the b-Si synthesized with various etching time and $HF : H_2O_2 : H_2O$ ratios. On the Si wafer surface, only few Ag NPs can be observed since most of them have sunk into the bottom of the nanopores. It is important to note that the diameter and length of the nanopores synthesized with lower [HF] and [H_2O_2] are smaller compared to those synthesized with higher [HF] and [H_2O_2] for the same allotted time. This phenomenon is attributed to the lower [H_2O_2] system requiring more time to grow the Ag NPs, which function as the catalysts for Si etching. Thus, the formation of nanopores is delayed, as well as both the nanopore diameter and length are directly affected. For example, as the etching time reaches 10 min, the maximum nanopore synthesized with the $HF : H_2O_2 : H_2O$ ratio of 1 : 5 : 2 has dimensions of 230 nm (diameter) and 4.1 μm (length), see Fig. 3a and b. These are much larger than those synthesized at the same etching time using a ratio of 1 : 5 : 20 whose diameter = 140 nm and length = 380 nm (Fig. 3e and f).

With a concentration of silver is 50 μM, the Si etching time also plays an important role in the structure of the etched surface. Over time the nanopores become larger and longer on the Si wafer surface (Fig. 3e–h). The growth of nanopores in the vertical direction is not difficult to understand because the Ag NPs continue catalyzing the Si etching under the NPs to increase the nanopore length, as long as the HF and H_2O_2 are sufficient in the etchant. The growth of nanopore diameter may be attributed to the presence of the dopant within the Si wafer. For the two-step Ag-assisted chemical etching, Zhong *et al.* proposed that some Ag ions diffuse upward from the pre-deposited Ag NPs at the nanopore bottom and re-nucleate at the defective sites around the dopant along the nanopore sidewalls.[28] The newly formed Ag nuclei trigger new Si etching processes on the nanopore sidewalls and increase the nanopore diameter and the porosity of sidewalls as well. Since the dopant concentration is higher on the wafer surface, the nanopores usually possess larger diameters at their surface end, resulting in an upside down cone shape. In the one-step Ag-assisted chemical etching method, we can infer that the change of nanopore diameter might be more significant than the two-step method since the Ag ions nucleating at the sidewall would come from not only the existed Ag NPs at the nanopore bottoms but also the Ag ions in the Si etchant.

It has been previously shown that the porous etching is related to the dopant type and dopant concentration in the Si wafer. With regard to the doping type, Zhang *et al.* reported that etching rate of an n-type Si wafer (7–13 Ω) is faster than that of a p-type Si wafer (7–13 Ω).[29] They also found that this occurs for both (100) and (111) substrates. With regard to the dopant concentration,[28] it was found that the nanopore becomes shorter with increasing dopant concentration. According to SEM studies it is proposed that the Ag nanoparticles at the nanopore bottom can be oxidized by H_2O_2 to form Ag^+ ions again, which may diffuse and renucleate on the nanopore sidewalls. The higher the dopant concentration the more the Ag clusters are proposed to re-nucleate at the nanopore sidewalls, and then less Ag nanoparticles are left at the nanopore bottom. This results in a slowing of the etching rates along the vertical direction and consequently shorten the nanopore length.

Another observation from the images in Fig. 3 that seems not able to be well described by the Zhong mechanism[28] is that the number of the nanopores decreases with the etching time (Fig. 3e–h). We have found that sonication resulted in more

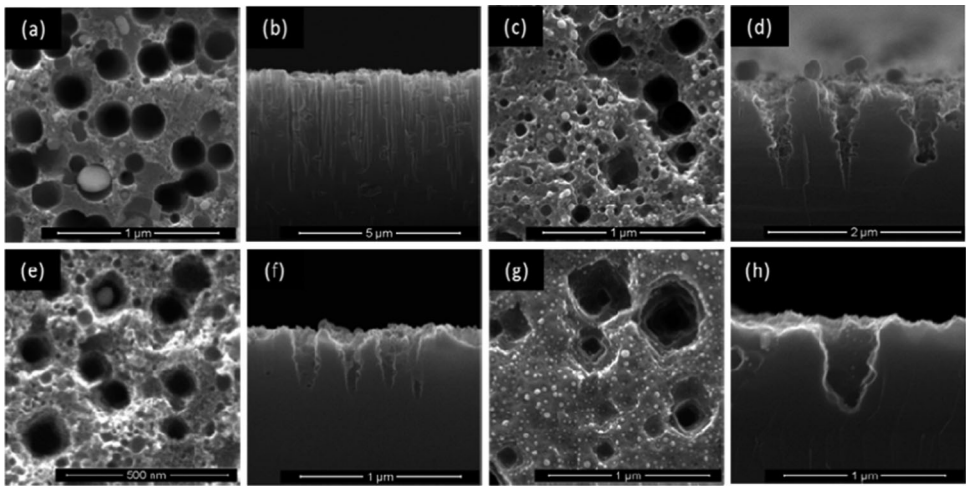

Fig. 3 SEM images of the morphology of b-Si synthesized by the Si etchant containing [Ag^+] = 50 μM with various etching time and $HF : H_2O_2 : H_2O$ ratios. Top views: (a) 10 min, 1 : 5 : 2, (c) 10 min, 1 : 5 : 10, (e) 10 min, 1 : 5 : 20, (g) 20 min, 1 : 5 : 20. Cross views: (b) 10 min, 1 : 5 : 2, (d) 10 min, 1 : 5 : 10, (f) 10 min, 1 : 5 : 20, (h) 20 min, 1 : 5 : 20. Note: the magnification of each image is chosen for clarity. Scale bars = 1 μm (a, c, f, g, and h), 5 μm (b), 2 μm (d) and 500 nm (e).

uniform size distribution of the nanopores on the Si wafer surfaces. We propose a possible mechanism that explains the decrease in nanopores as a function of etch time that includes the sonication. Fig. 4 shows a schematic summary for the formation of nanopores on a Si wafer surface through the one-step Ag-assisted chemical etching method with sonication. Initially, numerous Ag NPs with different sizes are deposited on the wafer surface and fabricate lots of nanopores with different diameter and length (Fig. 4a). However, there is also a thin layer of fine etched material that is easily removed by sonication during the etching reaction (Fig. 4b). Thus, the shallow nanopores are removed with the top surface and only larger and longer nanopores are left on the Si wafer. This results in some of the Ag NPs originally at the nanopore bottoms to partially emerge on the surface again and explains why the number of nanopores on the wafer surface significantly decreases with the etching time. At the same time, the Ag ions in the etchant aggregate on the re-emerged Ag NPs to form larger NPs because the Ag NPs on the wafer surface can transfer negative charges from the Si to the Ag ions for Ag formation; also, the total free energy of the Ag NP surfaces would be effectively decreased (Fig. 4c). With larger Ag NPs, nanopores with larger diameters are formed since the nanopores are the sinking tracks of Ag NPs. After a certain period of time, the Ag NPs have sunk too deeply to effectively attract the Ag ions. Hence, many newly formed small Ag NPs deposit on the top Si wafer surface instead of on the Ag NPs at the nanopore bottoms (Fig. 3g and 4d). This proposed mechanism explains the observation that the number of nanopores decreases with the etching time; however, for the growth of nanopore diameter, both our mechanism and the Zhong mechanism may need to be taken into consideration.

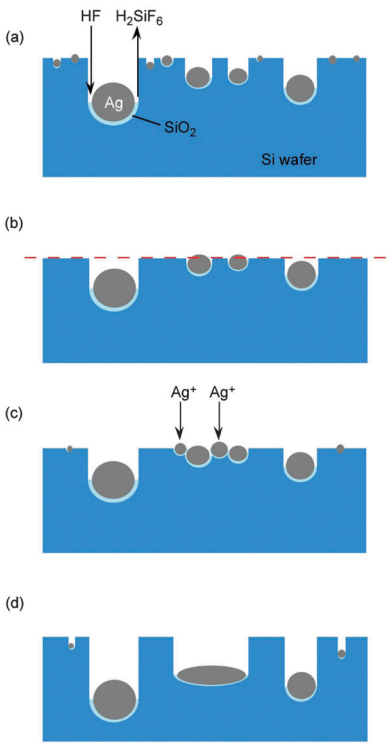

Fig. 4 Schematic illustration of the proposed formation process of large nanopores on the surface of the Si wafer during the one-step Ag-assisted chemical etching method with sonication: (a) nanopores are formed on the Si surface, (b) loose fragments are removed by sonication, (c) new Ag NP deposit near existing NPs, and (d) larger Ag NPs are formed and produce nanopores with larger diameters.

It is also worth mentioning that as the [HF] and [H_2O_2] in the etchant decrease, the shapes of nanopores change from circles to squares (*e.g.*, Fig. 3a, c and e). A possible explanation is that as the [HF] and [H_2O_2] are higher, the Si etching rate is relatively faster, so the Si under the Ag NPs can be easily etched and form the circular nanopores which are projected outlines of the NPs on the Si wafer surface. Nevertheless, when the [HF] and [H_2O_2] decrease, the Si etching rate slows down leading that the SiO_2 formation and the etching processes prefer to occur along the direction of Si–Si bonding because the bonding possesses a higher free energy and is favorable for the chemical reactions. Since the network of Si–Si bonding of the (100) Si wafer surface is square, the obtained outlines of nanopores from the chemical etching are consequently square as well.

Further decreasing the [Ag^+] to 5 μM maintains the formation of nanopores on the Si wafer surface, but the nanopores have smaller diameters and shorter lengths compared to those synthesized with the 50 μM [Ag^+] for the same etching conditions (see Fig. 3 and 5). For instance, with an etching time of 10 min, the maximum diameter and length of nanopores synthesized with 5 μM [Ag^+] and HF : H_2O_2 : H_2O ratio of 1 : 5 : 2 is 180 nm and 2.4 μm, respectively, *versus* 230 nm and 4.1 μm for those synthesized with 50 μM [Ag^+]. The reason is that the lower [Ag^+] system needs more time to grow Ag NPs for the Si etching, thus, it delays the formation of nanopores, as well as effects the size of the nanopores. In addition, with the slower rate of Ag NP formation, the nanopore size is more uniform and better controlled since the difference in size between each Ag NP is smaller. Fig. 5 shows SEM images of the morphology of the Ag-removed b-Si synthesized by the Si etchant containing 5 μM Ag ions for 10 minutes etching and various HF : H_2O_2 : H_2O ratios. Similar to the b-Si synthesized with 50 μM [Ag^+], the nanopore size on the b-Si synthesized with 5 μM [Ag^+] decreases as the concentration of HF and H_2O_2 decrease as well. After 10 minutes etching, the maximum nanopore diameter and length of the b-Si fabricated with HF : H_2O_2 : H_2O ratio of 1 : 5 : 20 is only around 70 nm and 90 nm, respectively (Fig. 5e and f). This once again shows that [HF] and [H_2O_2] significantly effect on Ag NP growth that has a direct relation with the nanopore formation.

The relative ratio of HF : H_2O_2 is also an important parameter for nanopore formation of the b-Si. Fig. 6 shows SEM images of the surface morphology synthesized with 5 μM [Ag^+] and the different relative ratios of HF : H_2O_2. From Fig. 6, it can be seen that the diameters of nanopore decrease with the volume portion of H_2O_2. The lower the H_2O_2 concentration in the Si etchant the smaller the Ag NPs that are formed, and consequently smaller nanopores. As the HF : H_2O_2 : H_2O ratio reaches 5 : 1 : 20, almost all the nanopores on the Si wafer surface are mesopores (2–50 nm) and the nanopore size distribution is decently uniform (Fig. 6g).

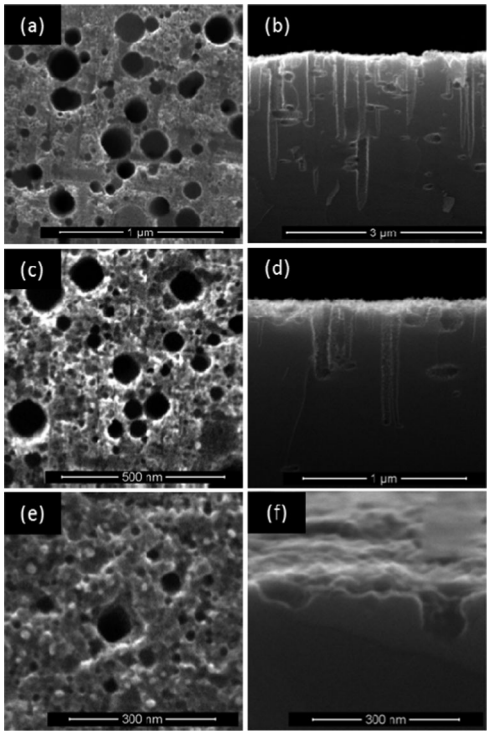

Fig. 5 SEM images of the morphology of b-Si samples synthesized by the Si etchant containing 5 μM [Ag^+] with 10 minutes etching and various HF : H_2O_2 : H_2O ratios. Top views: (a) 10 min, 1 : 5 : 2, (c) 10 min, 1 : 5 : 10, (e) 10 min, 1 : 5 : 20. Cross views: (b) 10 min, 1 : 5 : 2, (d) 10 min, 1 : 5 : 10, (f) 10 min, 1 : 5 : 20. Note: the magnification of each image is chosen for clarity of the feature of interest. Scale bars = 1 μm (a and d), 3 μm (b), 500 nm (c), and 300 nm (e and f).

The H_2O_2 in the etchant not only helps the formation of Ag nanoparticles but also assisted the oxidation of Si under the Ag nanoparticles (eqn (5)). The SEM image shown in Fig. 7 is of a sample prepared with 10 minute etching using a solution comprising 5 μM [Ag^+] and a ratio of HF : H_2O_2 : H_2O = 6 : 0 : 20. As we can see, without H_2O_2 there only few Ag nanoparticles deposited on the Si wafer, which results in the Si wafer surface

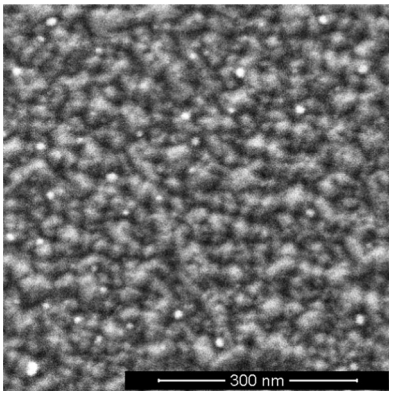

Fig. 7 SEM image of the morphology of b-Si surface synthesized by the Si etchant containing 5 μM [Ag^+] with 10 minute etching and a HF : H_2O_2 : H_2O = 6 : 0 : 20.

with a low-level texturized surface. This is despite a concentration of HF being sufficient to act as an etchant. This image proves that the addition of H_2O_2 is beneficial for the nanopore formation.

When the relative ratio of HF : H_2O_2 increases and the overall HF : H_2O_2 : H_2O ratio is 3 : 3 : 20, the nanopore length reaches its maximum (690 nm) for 10 minute etching time (Fig. 6d). However, if the relative ratio of HF : H_2O_2 is further increased, the nanopore length decreases and finally reaches its maximum of 250 nm with a ratio of HF : H_2O_2 : H_2O of 5 : 1 : 20. A possible explanation of this result is that the equivalent volume ratio of HF : H_2O_2 (*i.e.*, 3 : 3 : 20) can provide sufficient H_2O_2 for SiO_2 formation and sufficient HF for SiO_2 etching in order for the reactions to occur simultaneously. If the HF concentration is relatively low (*i.e.*, HF : H_2O_2 : H_2O = 1 : 5 : 20) the HF in the etchant is not sufficient to immediately remove the as-formed SiO_2 under the Ag NPs; conversely when the H_2O_2 concentration is relatively low (*i.e.*, HF : H_2O_2 : H_2O = 5 : 1 : 20) the H_2O_2 in the etchant is not sufficient to immediately oxidize the Si under the Ag NPs into SiO_2 for the consequent etching.

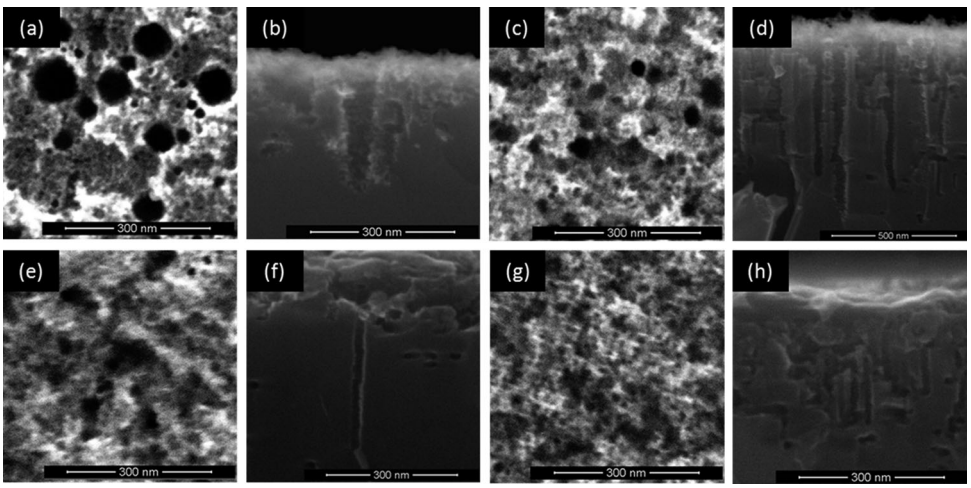

Fig. 6 SEM images of the morphology of b-Si synthesized by the Si etchant containing 5 μM [Ag^+] with 10 minute etching and various HF : H_2O_2 : H_2O ratios. Top views: (a) 2 : 4 : 20, (c) 3 : 3 : 20, (e) 4 : 2 : 20, (g) 5 : 1 : 20. Cross views: (b) 2 : 4 : 20, (d) 3 : 3 : 20, (f) 4 : 2 : 20, (h) 5 : 1 : 20. Scale bars = 300 nm.

Both extremes result in a slowing the etch rate and a decrease in the length of the pores.

Interestingly, the growth of nanopores is limited if the sonication treatment is not utilized during the Si etching. Without sonication, the nanopore length observed is significantly shorter compared to the ones etched with sonication treatment causing no nanopores can be clearly observed from the cross-sectional SEM images. This indicates the growth of nanopore length is suppressed more significantly than the growth of nanopore diameter in the absence of sonication. Furthermore, this result provides strong evidence that the sonication treatment can assist the HF and Ag ions to diffuse into the nanopore, effectively increasing the etching rate.

The morphology of b-Si directly affects the anti-reflection abilities. After the Ag NPs on the Si wafer surface are removed *via* the Ag etchant (see Experimental), the relative reflectivity of b-Si is measured for the light wavelengths of 300–1000 nm and compared to the cleaned and un-etched Si wafer whose relative reflectivity is set as 100.00%. A plot of the relative reflectivity as a function of wavelength is shown in Fig. 8. As may be seen the reflectivity is highly uniform across a wide range of wavelengths, in particular across the solar spectrum. A summary of the relative effective reflectivity for the samples is given in Table 2. There is a question as to whether our treatment results in a b-Si surface or simply a textured surface. The shape of our relative reflectivity curves (Fig. 8) show the same trend and shape (*i.e.*, higher reflectivity at higher wavelength for incomplete b-Si formation) as those reported by Branz *et al.*,[26] as well as well defined porous Si anti-reflection layers prepared by other routes.[30,31]

In order to graphically compare the various catalyst:etch treatments the relative effective reflectivity was categorized into five groups (<5, 5–10, 10–25, 25–50, 50–100). Fig. 9 shows the relative effective reflectivity of b-Si samples synthesized with different etching conditions. Generally, the relatively reflectivity of all samples decreases with etching time due to the longer nanopores. The longer nanopores provide a slower gradient change of refractive index within the b-Si surface; hence, they can more effectively suppress the reflection on the Si wafer surfaces.

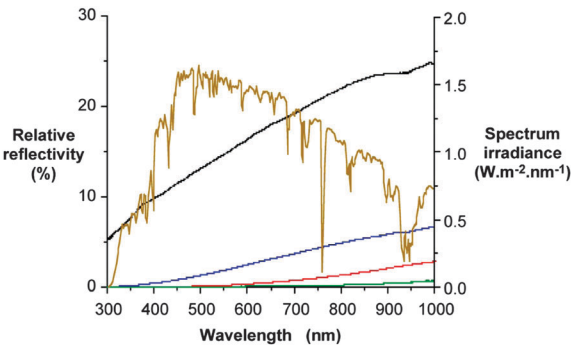

Fig. 8 Plot of relative reflectivity for b-Si formed using $[Ag^+]$ = 50 μM, with a $HF:H_2O_2:H_2O$ ratio of 1 : 5 : 2, and an etching time of 2 min (black), 5 min (blue), 10 min (red), and 20 min (green), the solar spectrum is overlain (yellow).

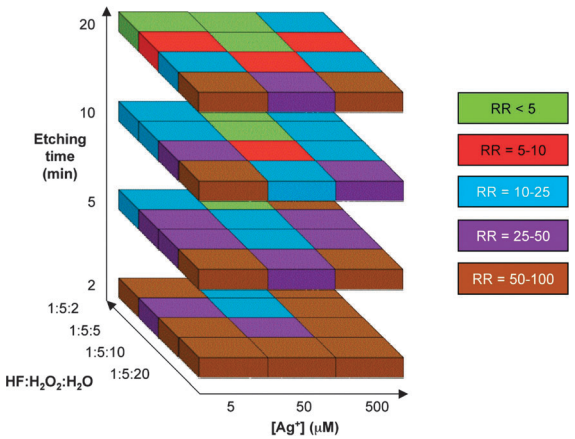

Fig. 9 Schematic plot of the relative effective reflectivity of b-Si with various $[Ag^+]$, etching time, and $HF:H_2O_2:H_2O$ ratio as $1:5:Z$.

When the silver concentration is 500 μM, all the relative effective reflectivity of sample is above 5% because only shallow pits are formed on the Si surfaces. However, the shallow pits also become deeper with time and make the surface rougher which still suppresses the reflection of wafer surface in a certain level (see Table 2). As compared to the b-Si synthesized with $[Ag^+]$ = 500 μM, the samples synthesized with $[Ag^+]$ = 50 μM show much better AR properties. With 50 μM $[Ag^+]$, the nanopores are formed on the Si surface and grow with the etching time allowing the b-Si samples to possess extremely low reflectivity. As the HF and H_2O_2 concentrations increase, the formed nanopores become longer which further lowers the reflectivity of the wafer surfaces. For example, the b-Si synthesized with 20 minute etching and the $HF:H_2O_2:H_2O$ ratio of 1 : 5 : 2 shows an relative effective reflectivity of 0.17%, which is the lowest of the samples studied. For the b-Si synthesized with the same $[Ag^+]$ and etching time but different $HF:H_2O_2:H_2O$ ratios, the relative effective reflectivity increases with lower [HF] and $[H_2O_2]$, see Table 2.

The b-Si fabricated with $[Ag^+]$ = 5 μM effectively decreases the reflection of the Si wafer surface as well. However, the relative effective reflectivity is lower than the ones fabricated with 50 μM $[Ag^+]$ because of the shorter nanopore length. The relative effective reflectivity also decreases with the etching time, similar to the b-Si fabricated with 50 μM $[Ag^+]$. With etching time of 10 minutes, the relative effective reflectivity increases with increased dilution (*i.e.*, lower [HF] and $[H_2O_2]$), see Table 2. A similar trend is observed for 20 min etching as well.

It was also found that the relative effective reflectivity decreases as the relative ratio of $HF:H_2O_2$ increases (Fig. 10). With etching time of 10 minutes, the relative effective reflectivity decreases with increased $HF:H_2O_2$ ratio (*i.e.*, decreased $[H_2O_2]$). This indicates that when the nanopores are short, the effect of nanopore length on reflectivity becomes less significant, and the nanopore size uniformity starts to dominate the reflectivity. Typically, a p–n junction interface in a Si-based solar cell is about 500 nm below the Si wafer top surface. The maximum nanopores length of b-Si synthesized with the 5 μM $[Ag^+]$ and $HF:H_2O_2:H_2O$ ratio of 5 : 1 : 20 is only around 250 nm, this indicates the synthesized b-Si is favorable for

Table 2 Summary of relative reflectivity data for b-Si samples

$[Ag^+]$ (μM)	$X:Y:Z$ ($HF:H_2O_2:H_2O$)	Time (min)	Relative reflectivity @ 300.16 nm (%)	Relative reflectivity @ 999.64 nm (%)	Relative effective reflectivity (%)
500	1:5:2	2	76.123	91.014	88.492
500	1:5:2	5	42.308	76.226	69.504
500	1:5:2	10	12.614	29.252	23.949
500	1:5:2	20	5.292	22.878	14.787
500	1:5:5	2	65.766	84.753	78.940
500	1:5:5	5	27.445	46.494	38.739
500	1:5:5	10	12.294	24.383	21.541
500	1:5:5	20	5.771	8.036	7.397
500	1:5:10	2	57.322	76.620	68.663
500	1:5:10	5	24.828	35.536	31.854
500	1:5:10	10	16.449	21.464	19.447
500	1:5:10	20	11.541	16.528	14.671
500	1:5:20	2	75.402	92.592	87.626
500	1:5:20	5	87.407	97.941	94.250
500	1:5:20	10	34.104	42.573	38.065
500	1:5:20	20	47.386	64.157	61.203
50	1:5:2	2	5.281	24.673	17.208
50	1:5:2	5	0.019	6.605	3.187
50	1:5:2	10	0.001	2.821	0.872
50	1:5:2	20	0.000	0.695	0.167
50	1:5:5	2	8.954	30.242	22.774
50	1:5:5	5	1.654	17.886	10.618
50	1:5:5	10	0.042	8.306	3.542
50	1:5:5	20	0.001	2.892	0.948
50	1:5:10	2	23.047	50.527	40.022
50	1:5:10	5	3.764	27.741	18.003
50	1:5:10	10	0.361	21.047	9.996
50	1:5:10	20	0.239	14.152	5.142
50	1:5:20	2	65.372	93.377	78.307
50	1:5:20	5	11.555	40.249	30.849
50	1:5:20	10	4.304	37.048	23.955
50	1:5:20	20	3.244	42.619	25.295
5	1:5:2	2	54.052	68.603	57.190
5	1:5:2	5	4.348	26.330	17.229
5	1:5:2	10	2.525	24.824	15.003
5	1:5:2	20	0.233	12.193	4.976
5	1:5:5	2	32.938	63.114	46.817
5	1:5:5	5	17.032	42.904	33.082
5	1:5:5	10	7.309	37.176	24.706
5	1:5:5	20	0.772	18.852	9.138
5	1:5:10	2	63.805	83.982	68.122
5	1:5:10	5	22.961	59.344	42.181
5	1:5:10	10	12.366	43.298	31.238
5	1:5:10	20	3.284	32.417	18.983
5	1:5:20	2	92.404	90.141	92.505
5	1:5:20	5	45.069	83.930	65.290
5	1:5:20	10	49.496	79.739	67.578
5	1:5:20	20	32.260	75.665	54.144
5	2:4:20	2	89.406	89.337	90.721
5	2:4:20	5	13.974	49.764	33.879
5	2:4:20	10	9.610	33.164	25.441
5	3:3:20	2	39.943	72.919	55.647
5	3:3:20	5	14.241	39.018	29.213
5	3:3:20	10	2.829	19.114	10.716
5	4:2:20	2	54.280	71.223	56.416
5	4:2:20	5	8.766	39.533	23.004
5	4:2:20	10	2.561	16.817	8.258
5	5:1:20	2	66.124	71.809	64.679
5	5:1:20	5	8.007	36.272	21.453
5	5:1:20	10	0.520	4.625	2.599

the anti-reflection layer of Si-based solar cells. With these extremely short nanopores, the p–n junction interface will not be destroyed by the nanopore structures during the fabrication process of anti-reflection layer *via* the one-step Ag-assisted chemical etching.

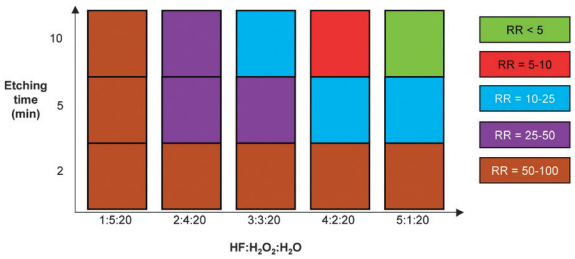

Fig. 10 Plot of the relative effective reflectivity of b-Si with 5 μM $[Ag^+]$ and various etching time and $HF:H_2O_2:H_2O$ ratio as $X:Y:20$.

4. Conclusion

The one-step Ag-assisted chemical etching method we used is a simple and economical technique for rapidly synthesizing nanopore-type b-Si. Our results indicate that the b-Si morphology, which directly affects the reflectivity degree, possesses high dependence on the $[Ag^+]$, the $HF:H_2O_2:H_2O$ volume ratio, and the etching time. The lowest relative effective reflectivity of b-Si that we obtained is 0.17% with the $HF:H_2O_2:H_2O$ ratio of 1:5:2 and $[Ag^+]$ = 50 μM. By adjusting the $HF:H_2O_2:H_2O$ ratio to 5:1:20, we can even use further lower $[Ag^+]$, 5 μM, to fabricate the b-Si whose relative effective reflectivity still reaches 2.60%.

Our b-Si structure with smallest nanopore diameter (<30 nm) and shortest nanopore length (<250 nm) are similar to the structures synthesized by Branz *et al.* using a gold-assisted chemical etching.[26] While, the relative effective reflectivity of this structure (2.60%) is not the lowest of our b-Si samples (0.17%), it is comparable to their lowest effective reflectivity for the similar sized features.[26]

We propose that the simplicity of the process and low reaction times, along low consumption of silver precursor will make such a one-step method scalable for industrial applications where process cost and rate are important. Moreover, the nanopore length of b-Si fabricated with 5 μM $[Ag^+]$ can be controlled to be around 250 nm, which is shorter than a typical p–n junction depth in Si-based solar cells, and would not interfere with the function of the cell.

A comparison of our b-Si structures to those reported by Branz and co-workers for multi-step processes[27] show that both of the b-Si materials have the similar morphology; the nanopore lengths are both under 500 nm and nanopore diameters are both under 100 nm. This implies that our black Si is also potential to be used in Si-based solar cells for obtaining high-energy conversion efficiency. However, our fabrication process based on one-step silver-assisted chemical etching is less complicated than the multi-step process, which is based on a two-step silver-assisted chemical etching that still needs the extra third step to modify the nanopore length. More importantly we have shown the relationship of silver concentration to the morphology of the b-Si, and that the concentration of $AgNO_3$ that we used for Ag nanoparticle formation (5 and 50 μM) is much lower than the concentration for the multi-step process (1 mM). This shows our fabrication process of

black Si is simple and economical. Also, the reflectivity of our black Si is comparable to, or even lower than that of multi-step process, which is between 2–12% depending on TMAH etching time.

Acknowledgements

This work was supported by Natcore Technology, Inc. (NXT.V) and the Robert A. Welch Foundation (C-0002). The authors thank Prof. S. Curran (University of Houston) for the assistance of the b-Si reflectivity measurement.

Notes and references

1 S. Walheim, E. Schaffer, J. Mlynek and U. Steiner, *Science*, 1999, **283**, 520–522.
2 M. L. Kuo, D. J. Poxson, Y. S. Kim, F. W. Mont, L. K. Kim, E. F. Schuhert and S. Y. Lin, *Opt. Lett.*, 2008, **33**, 2527–2529.
3 S.-S. Lo, C.-C. Chen, F. Garwe and T. Pertch, *J. Phys. D: Appl. Phys.*, 2007, **40**, 754–758.
4 L. L. Ma, Y. C. Zhou, N. Jiang, X. Lu, J. Shao, W. Lu, J. Ge, X. M. Ding and X. Y. Hou, *Appl. Phys. Lett.*, 2006, **88**, 171907.
5 H. Jansen, M. de Boer, R. Legtenberg and M. Elwenspoek, *J. Micromech. Microeng.*, 1995, **5**, 115–120.
6 Y. Liu, T. Lai, H. Li, Y. Wang, Z. Mei, H. Liang, Z. Li, F. Zhang, W. Wang, A. Y. Kuznetsov and X. Du, *Small*, 2012, **8**, 1392–1397.
7 K. Peng, Y. Xu, Y. Wu, Y. Yan, S.-T. Lee and J. Zhu, *Small*, 2005, **1**, 1062–1067.
8 K. Peng, X. Wang and S. T. Lee, *Appl. Phys. Lett.*, 2008, **92**, 163103.
9 S. Chattopadhyay, Y. F. Huang, Y. J. Jen, A. Ganguly, K. H. Chen and L. C. Chen, *Mater. Sci. Eng., R*, 2010, **69**, 1–35.
10 A. A. Ayon, R. Braff, C. C. Lin, H. H. Sawin and M. A. Schmidt, *J. Electrochem. Soc.*, 1999, **146**, 339–349.
11 Y. Hirai, H. Yabu, Y. Matsuo, K. Ijiro and M. Shimomura, *J. Mater. Chem.*, 2010, **20**, 10804–10808.
12 T. H. Her, R. J. Finlay, C. Wu, S. Deliwala and E. Mazur, *Appl. Phys. Lett.*, 1998, **73**, 1673–1675.
13 H. Mei, C. Wang, J. Yao, Y. C. Chang, J. Cheng, Y. Zhu, S. Yin and C. Luo, *Opt. Commun.*, 2011, **284**, 1072–1075.
14 C. Wu, C. H. Crouch, L. Zhao, J. E. Carey, R. Younkin, J. A. Levinson, E. Mazur, R. M. Farrell, P. Gothoskar and A. Karger, *Appl. Phys. Lett.*, 2001, **78**, 1850–1852.
15 R. R. Bilyalov, L. Stalmans, L. Schirone and C. Levy-Clement, *IEEE Trans. Electron Devices*, 1999, **46**, 2035–2040.
16 Y. Kanamori, M. Sasaki and K. Hane, *Opt. Lett.*, 1999, **24**, 1422–1424.
17 X. Li and P. W. Bohn, *Appl. Phys. Lett.*, 2000, **77**, 2572–2574.
18 K. Peng, Z. Huang and J. Zhu, *Adv. Mater.*, 2004, **16**, 73–76.
19 C. Chartier, S. Bastide and C. Levy-Clement, *Electrochim. Acta*, 2008, **53**, 5509–5516.
20 S. K. Srivastava, D. Kumar, P. K. Singh, M. Kar, V. Kumar and M. Husain, *Sol. Energy Mater. Sol. Cells*, 2010, **94**, 1506–1511.
21 K. Peng, Y. Wu, H. Fang, X. Zhong, Y. Xu and J. Zhu, *Angew. Chem., Int. Ed.*, 2005, **44**, 2737–2742.
22 K. Peng, J. Hu, Y. Yan, Y. Wu, H. Fang, Y. Xu, S. T. Lee and J. Zhu, *Adv. Funct. Mater.*, 2006, **16**, 387–394.
23 K. Peng, A. Lu, R. Zhang and S. T. Lee, *Adv. Funct. Mater.*, 2008, **18**, 3026–3035.
24 T. Tsuboi, T. Sakka and Y. H. Ogata, *J. Appl. Phys.*, 1998, **83**, 4501–4506.
25 X. H. Xia, C. M. A. Ashruf, P. J. French and J. J. Kelly, *Chem. Mater.*, 2000, **12**, 1671–1678.
26 H. M. Branz, V. E. Yost, S. Ward, K. M. Jones, B. To and P. Stradins, *Appl. Phys. Lett.*, 2009, **94**, 231121.
27 J. Oh, H.-C. Yuan and H. M. Branz, *Nat. Nanotechnol.*, 2012, **7**, 743–748.
28 X. Zhong, Y. Qu, Y. C. Lin, L. Liao and X. Duan, *ACS Appl. Mater. Interfaces*, 2011, **3**, 261–270.
29 M.-L. Zhang, K.-Q. Peng, X. Fan, J.-S. Jie, R.-Q. Zhang, S.-T. Lee and N.-B. Wong, *J. Phys. Chem. C*, 2008, **112**, 4444–4450.
30 S. K. Sirvastava, D. Kumar, P. K. Singh, M. Kar, V. Kumar and M. Husain, *Sol. Energy Mater. Sol. Cells*, 2010, **94**, 1506–1511.
31 Y. Liu, T. Lai, H. Li, Y. Wang, Z. Mei, H. Liang, Z. Li, F. Zhang, W. Wang, A. Y. Kuznetsov and X. Du, *Small*, 2012, **8**, 1392–1397.

